The Role of Sediment-induced Light Attenuation on Primary Production during Hurricane Gustav (2008)

Zhengchen Zang[1, +], Z. George Xue[1,2,3 *], Kehui Xu [1,3], Samuel J. Bentley [3,4], Qin Chen[5], Eurico J. D'Sa[1,3], Le Zhang[1], Yanda Ou[1]

[1] Department of Oceanography and Coastal Sciences, Louisiana State University, Baton Rouge, LA 70803, USA

[+] current address: Department of Biology, Woods Hole Oceanographic Institution, Woods Hole, MA, 02543

[2] Center for Computation and Technology, Louisiana State University, Baton Rouge, LA 70803, USA

[3] Coastal Studies Institute, Louisiana State University, Baton Rouge, LA 70803, USA

[4] Department of Geology and Geophysics, Louisiana State University, Baton Rouge, LA 70803, USA

[5] Department of Civil and Environmental Engineering, Northeastern University, Boston, MA 02115, USA

Corresponding author: Z. George Xue (zxue@lsu.edu)

Key Words:

Gulf of Mexico; Sediment-induced light attenuation; hurricane; offshore bloom.

Abstract

We introduced a sediment-induced light attenuation algorithm into a biogeochemical model of the Coupled Ocean-Atmosphere-Wave-Sediment Transport (COAWST) modeling system. A fully coupled ocean-atmospheric-sediment-biogeochemical simulation was carried out to assess the impact of sediment-induced light attenuation on primary production in the northern Gulf of Mexico during the passage of Hurricane Gustav in 2008. When compared with model results without sediment-induced light attenuation, our new model showed a better agreement with satellite data on both the magnitude of nearshore chlorophyll concentration and the spatial distribution of offshore bloom. When Gustav approached, resuspended sediment shifted the inner shelf ecosystem from a nutrient-limited one to light-limited. One week after Gustav's landfall, accumulated nutrient and favorable optical environment induced a post-hurricane algal bloom in the top 20 m of water column, while the productivity in the lower water column was still light-limited due to slow-settling sediment. Corresponding with the elevated offshore NO_3 flux (38.71 mmol N/m/s) and decreased chlorophyll flux (43.10 mg/m/s), the outer shelf post-hurricane bloom should be resulted from the cross-shelf nutrient supply instead of the lateral dispersed chlorophyll. Sensitivity tests indicated that sediment light attenuation efficiency affected primary production when sediment concentration was moderately high. Model uncertainties due to colored dissolved organic matter and parameterization of sediment-induced light attenuation are also discussed.

1 Introduction

Light, nutrient and temperature play a vital role in photosynthesis and marine ecosystems. The vertical structure of light availability in an aquatic environment is mainly modulated by the shading effects of chlorophyll, colored dissolved organic matter (CDOM), detritus, and sediment (Cloern, 1987; Devlin et al., 2008; Schaeffer et al., 2011; Ganju et al., 2014; McSweeney et al., 2017). The optical environment in river-dominated shelves are more complex due to the interaction between riverine inputs and regional hydrodynamics (Bierman et al., 1994; Lin et al., 2009; Zhu et al., 2009). As the largest river in North America, the Mississippi-Atchafalaya River system delivers 380 km^3 of freshwater and 115 Mt of sediments each year into the northern Gulf of Mexico (nGoM; Meade and Moody, 2010; Allison et al., 2012). Along the Louisiana-Texas shelf in the nGoM, suspended sediment concentration (SSC) in the water column exhibits strong seasonality: high in winter and spring seasons due to strong sediment resuspension and high fluvial sediment discharge, while largely reduced in summer and fall owing to the relatively low river inputs and weak resuspension (Zang et al., 2019). Episodic hurricane events in summer and fall can disturb vertical stratification and resuspend large amount of shelf sediment (D'Sa et al., 2011; Xu et al., 2016; Zang et al., 2018). Enhanced resuspension during a hurricane might greatly change the shelf ecosystem via modifying light availability. In addition, enhanced organic matter remineralization in the bottom boundary layer could also introduce sharp changes to the ecosystem (Wilson et al., 2013; Hurst et al., 2019). Yet studies of the impact from hurricane-induced resuspension are still limited due to the challenge of *in-situ* data collection under extreme weather conditions.

As an alternative tool to fill the spatial and temporal gaps in *in-situ* datasets, coupled physical-biogeochemical models have been widely applied to the Gulf of Mexico (GoM; e.g., Fennel et al., 2008; Laurent et al., 2012; Xue et al., 2013; Yu et al., 2015; Gomez et al., 2018). In these models, photosynthetically available radiation was estimated using a similar method, namely, light availability decreasing exponentially with water depth and the concentrations of light absorbers (e.g., sediment and CDOM) in the overlying water column. Due to the lack of long-term

observations of CDOM, however, its impact on the optical environment was either not included (e.g., Fennel et al., 2006; Gomez et al., 2018) or simply expressed as a function of salinity (Justić and Wang 2014). Although most of these studies considered sediment-induced light attenuation when estimating primary production, the related parameterization was uniform over the entire research domain and did not vary with sediment dynamics (e.g., Zhou et al., 2017; Thewes et al., 2020). Such an oversimplified treatment of sediment-induced light attenuation could substantially impact a model's robustness in river-dominated shelves that encompass a wide range of SSC. In the nGoM, Justić and Wang (2014) tentatively employed a new scheme by connecting sediment-induced light attenuation with river discharge (salinity) and hydrodynamics (bottom shear stress). However, the horizontal distribution of SSC in a realistic environment is not necessarily correlated with that of the freshwater plume, and the contribution of resuspension to SSC at different depths might be significantly different (Xu et al., 2011, 2016).

Gustav was the first major hurricane that made a landfall in Louisiana after Katrina (2005). It passed through the center of GoM and landed near Cocodrie, Louisiana on September 1st, 2008 as a Category 2 hurricane (Forbes et al., 2010). Sediment resuspension and transport were strong during the passage of Gustav, and thick post-hurricane deposition (up to 40 cm) was simulated on the inner shelf (Zang et al., 2018) and in the bays (Liu et al., 2018). Korobkin et al. (2009) identified a post-Gustav algal bloom around the Mississippi Delta on satellite images. High respiration and stratification after the landfall of Gustav was reported to be connected with possible hypoxia development on the shelf (McCarthy et al., 2013).

In this study, we introduce a new biogeochemical model with sediment-induced light attenuation to the three-way coupled (atmospheric-wave-ocean-sediment transport) Gustav model (Zang et al., 2018). While sediment dynamics can also impact nutrient dynamics via changing the intensity of remineralization near the bottom (Moriarty et al., 2018), the scope of this study is to investigate the influence of suspended sediment on the optical environment and thus primary production. The impact from elevated remineralization of resuspended particular organic matter during hurricane events is not considered as detailed processes because relevant parameterizations are still largely unknown. The objectives of this paper are to: 1) evaluate the impact of sediment-induced light attenuation on the spatiotemporal variation of nutrient-phytoplankton dynamics during a hurricane event; 2) explore the driving mechanism of the post-hurricane bloom on the shelf; and 3) investigate the response of primary production to sediment optical characteristics.

2 Model Description

2.1 Physical, sediment and biogeochemical models

Our model covered the entire GoM (Fig. 1a) and was built on the coupled ocean-atmosphere-wave-and-sediment transport (COAWST) modeling system (Warner et al., 2008, 2010). COAWST is an open source model platform that consists of three numerical models: the Weather Research and Forecasting model (WRF; Skamarock et al., 2005), the Regional Ocean Modeling System (ROMS; Shchepetkin and McWilliams, 2005; Haidvogel et al., 2008), and the Simulating Waves Nearshore model (SWAN; Booij et al., 1999). The Community Sediment Transport Modeling System (CSTMS) is included in ROMS to simulate sediment transport, stratigraphy, and geomorphology. Model Coupling Toolkit (MCT; Jacob et al., 2005) enables the interaction among these three models. The details of model setup and validation of the three-way coupled hydrodynamic-sediment transport model (WRF-ROMS-SWAN-CSTMS) were described in Zang et al. (2018), where four types of sediment (two cohesive and two non-cohesive) were defined with different grain diameters and settling velocities. There were 40 sediment layers on

the sea floor with a total thickness of 1 m to resolve sediment bed erosion and deposition. The driving force of sediment resuspension was determined by bottom shear stress induced by wave and current.

Given the importance of diatom in phytoplankton community in the nGoM (Zhao and Quigg, 2014), it is necessary to have both nitrogen and silicon cycles in the model. The biogeochemical model in this study was largely built on the North Pacific Ecosystem Model for Understanding Regional Oceanography (NEMURO; Kishi et al., 2007), which incorporated both nitrogen and silicon flows. There were 11 state variables included in the model: nitrate, ammonium, two types of phytoplankton (small and large), three types of zooplankton (microzooplankton, mesozooplankton and predatory zooplankton), particulate and dissolved nitrogen, particulate silica, and silicic acid concentration. River nutrient discharge during the hurricane were retrieved from United States Geological Survey (USGS) Water Data for the Nation website (http://nwis.waterdata.usgs.gov; Station 07374000). The growth of phytoplankton was driven by water temperature, light availability, and nutrient concentration. Instantaneous remineralization of particulate organic nitrogen at the bottom was estimated following Fennel et al. (2006). Our model did not include phosphate because its limitation on primary production in the nGoM was mainly between May to July (Laurent et al., 2012; Laurent and Fennel, 2014). We incorporated two types of chlorophyll corresponding to the large and small phytoplankton tracers, respectively. Following Fennel et al. (2006), chlorophyll dynamics was derived from phytoplankton equation by multiplying the ratio of chlorophyll to phytoplankton biomass. To get an ideal parameterization set and a stable initial condition for the biogeochemical variables, we first conducted a 20-yr (1993-2012) coupled physical-biogeochemical simulation using only ROMS model, where WRF and SWAN were disabled to achieve a feasible computation load (Step 1 in Fig. 2). The atmospheric forcing was provided by the 6-hourly, 38 km horizontal resolution Climate Forecast System Reanalysis (CFSR; Saha et al., 2010, 2011; http://cfs.ncep.noaa.gov). The physical setup of the 20-yr simulation was the same as Zang et al. (2019). The biogeochemical parameterizations (Table S1) were largely adapted after a recent GoM biogeochemical modeling study by Gomez et al. (2018). Since this study focused on the response of biogeochemical process to hurricane events, details of the 20-yr simulation setup and model-observation comparison were provided in the supplementary material. Once validated, the biogeochemical variables were extracted from the 20-yr model on August 30th, 2008 as the initial condition for this Gustav simulation (Step 2 in Fig. 2).

The light available for photosynthesis (I) is estimated using the following equation:

$$I = I_0 \cdot par \cdot exp\,\{-Z[\alpha_w + \alpha_{chl}\int_z^0 (PSn + PLn)dz + \alpha_{sed}\int_z^0 SSCdz]\},$$

where I_0 is the light intensity at the surface layer, and Z is water depth. par is the fraction of light available for photosynthesis (specified as 0.43). α_w and α_{chl} are the light attenuation coefficients of sea water and chlorophyll, respectively. PSn and PLn represent concentrations of small and large phytoplankton. Compared with the original biogeochemical model, we added a new sediment-induced light attenuation term in this equation. α_{sed} is the light attenuation coefficient due to suspended sediment, and SSC is total suspended sediment concentration in the respective layer. We performed a benchmark run ($\alpha_{\mathrm{sed}} = 0.059$; McSweeney et al., 2017) to represent the scenarios with sediment-induced light attenuation. The simulation period was from August 30th to September 10th, 2008.

2.2 Sensitivity tests

High turbidity in the Mississippi River Delta due to fluvial sediment discharge and resuspension suggested the vital role of sediment in the underwater optical environment. To quantitatively evaluate the importance of suspended sediment in light attenuation, we conducted a sensitivity test (test 1) without sediment-induced light attenuation ($\alpha_{sed} = 0$). Since the physical properties of a sediment particle (e.g., size, shape, roughness, and color) determine its light attenuation efficiency (Baker and Lavelle, 1984; Storlazzi et al., 2015), a wide range of α_{sed} has been applied in previous studies (e.g., Pennock, 1985; Arndt et al., 2007; McSweeney et al., 2017). Here we increased/decreased the benchmark α_{sed} (0.059) by 20% and 40% to examine the sensitivity of primary production to sediment-induced light attenuation (tests 2–5). The rest of the model setup were the same between the benchmark run and sensitivity tests (tests 1-5). The deviation due to the chaotic nature of turbulence was not considered in this study.

3 Model Validation

Direct measurements of ocean conditions during the passage of a hurricane are still challenging. In Zang et al. (2018) we validated the physical model's performance against the air pressure, sea level, and wave heights recorded at available buoy stations. The sediment model's performance was evaluated against satellite images. In this study, we used the five-day composites of SeaWiFS chlorophyll data (OC4) obtained before (Aug 25th–29th) and after (September 5th–9th) Gustav's landing to calibrate our biogeochemical model's initial condition and results. Surface chlorophyll distribution during initial condition (Fig. 3a) was similar to that in the pre-hurricane composite imagery (Fig. 3b), with high chlorophyll concentration (> 4 mg/m^3) located around the bird-foot delta and the Atchafalaya inner shelf, and values declined seaward to ~0.1 mg/m^3.

Compared with the pre-hurricane composite imagery, the post-hurricane composite showed higher chlorophyll concentration around the bird-foot delta and on the Atchafalaya shelf (Figs. 3b and 3c). Another major increase was identified in waters between the 50 and 200 m isobaths off the Atchafalaya Bay with chlorophyll concentration increasing from 1 to 4 mg/m^3 after Gustav, indicating a possible post-hurricane algal bloom on the outer shelf. When comparing with model run without sediment-induced attenuation, the intensity of the offshore bloom was better reproduced (~ 4 mg/m^3) with the new sediment-induced light attenuation algorithm (see difference between Figs. 3d and 3e). To quantitatively evaluate the model's performance, we calculated the root mean square error (RMSE) and correlation coefficient (R) between model-simulated and satellite-derived chlorophyll concentrations over the inner shelf (water depth < 50 m; Fig. 4). The reduced RMSE in the benchmark run in comparison to sensitivity test (2.33 to 1.91) suggested improved model performance with sediment-induced light attenuation. However, with only marginal differences in the correlation coefficients between the two experiments (0.82 and 0.81), the spatial distributions of chlorophyll were comparable (Fig. 4). Nevertheless, the model's performance in the high productivity waters (both simulated and observed chlorophyll concentrations > 1 mg/m^3) was significantly improved (R increased from 0.55 to 0.61, and RMSE decreased from 5.93 to 3.97; Fig. 4). The improvement of model results confirmed the importance of sediment-induced light attenuation in biogeochemical cycling during a hurricane event, particularly in coastal regions where chlorophyll concentration was high.

4 Results and Discussion

4.1 Temporal variability of biogeochemical variables

To examine the temporal variation of biogeochemical variables during the passage of Gustav, we plotted the time series of spatially averaged net primary production (growth of phytoplankton minus the respiratory losses; NPP), surface chlorophyll concentration, surface NO_3 concentration, SSC, downward solar short wave radiation, and sea surface temperature (SST) over the nGoM inner shelf (Fig. 5; < 50 m water depth). NPP exhibited strong diel variation and the peaks were strongly correlated with short wave radiation maximum (Figs. 5a and 5e). Such diel cycle could also be found in chlorophyll concentration, but with a 3- to 4-hour delay (Fig. 5b). Before the arrival of Gustav, daily-averaged NPP was around 0.05 g C/m^2/hr, and the differences of NPP and chlorophyll concentration between the benchmark run and test 1 were minor (Figs. 5a and 5b).

Following hurricane Gustav's landfall along coastal Louisiana at 16:00:00 UTC on September 1st, surface SSC increased to 3.8 kg/m^3 because of strong seabed resuspension (Fig. 5d). Daily-averaged NPP reduced to 0.03 g C/m^2/hr in test 1. Once sediment-induced light attenuation was included, daily-averaged NPP further declined to 0.01 g C/m^2/hr, suggesting that light availability severely limited short-term productivity on the inner shelf. Chlorophyll concentrations in the benchmark run and test 1 were reduced by 40% as Gustav approached. Hurricane-related surface cooling, together with decreased light (Figs. 5e and 5f), contributed to the reductions of both chlorophyll and NPP.

The difference of daily-averaged NPP between the benchmark run and test 1 maximized on September 2nd due to light limitation modulated by resuspended sediment (Figs. 5a and 5d). On September 3rd, daily-averaged NPP of test 1 recovered to 0.04 g C/m^2/hr and remained steady through the end of our simulation (Fig. 5a). For the benchmark run, however, the recovery of NPP was much slower: daily-averaged NPP was lower than that of test 1 until September 7th, when most suspended sediment settled back onto the seabed. NO_3 concentration went up gradually between September 2nd - 7th in the benchmark run (Fig. 5c) as nutrient consumption was constrained by the decline in photosynthetic activity. Accumulated NO_3, together with the improved optical environment due to low SSC, resulted in higher NPP and algal bloom after September 7th (Figs. 5a and 5b).

4.2 Vertical structure of biogeochemical variables

We extracted concentrations of chlorophyll, NO_3, sediment and water density anomaly along the transect D in Rabalais et al. (2001; Fig. 1b for transect location) at three time points (August 31st, September 2nd, and September 10th) to represent pre-, during-, and post-hurricane stages, respectively (Figs. 6 and 7). Before the approach of Gustav, offshore water was well stratified (Fig. 7d). Chlorophyll concentration decreased seaward from 5 to 0.3 mg/m^3 (Figs. 6a and 6d). Sediment-induced light attenuation did not alter the vertical structure of chlorophyll and NO_3 much (Figs. 6a, 6d, 6g, and 6j) owing to low SSC in the water column (Fig. 7a). On September 2nd, strong vertical mixing increased the SSC to more than 1 kg/m^3 over the entire water column (Figs. 7b and 7e). Chlorophyll concentration in waters < 40 m in the benchmark run was ~ 4 mg/m^3, lower than that in test 1 due to sediment-induced light attenuation (Figs. 6b and 6e). Higher NO_3 concentration in the benchmark run was a result of the weakened primary production and nutrient consumption (Figs. 6h and 6k). The most striking differences of chlorophyll and NO_3 between the two simulations were in water shallower than 20 m.

In test 1, chlorophyll concentration during the post-hurricane stage was lower than that of the pre-hurricane stage (Figs. 6a and 6c), in contrast to the condition captured by satellite imagery (Figs. 3b and 3c). The benchmark run, however, successfully reproduced the magnitude and

seaward extension of the post-hurricane bloom (Fig. 6f). High chlorophyll concentration (> 1 mg/m^3; Fig. 6f) with low NO_3 (Fig. 6l) was simulated in the top 20 m of the water column where stratification partially recovered (Fig. 7f) and sediment concentration was low after the passage of Gustav (Fig. 7c). At water deeper than 20 m, chlorophyll concentration dropped drastically to less than 0.1 mg/m^3, while NO_3 concentration further increased to > 1 $mmol/m^3$. The synchronized high turbidity and low chlorophyll concentration implied that, nine days after Gustav's landfall, the primary production in deeper water could still be constrained by light availability. A similar vertical structure (high SSC and low chlorophyll at the bottom) was also simulated in the Delaware estuary, where near bottom productivity was constrained by the estuarine turbidity maximum (McSweeney et al., 2017). Such a stratified water column with high/low productivity at the surface/bottom is generally favorable for bottom oxygen depletion. The elevated surface phytoplankton growth following the hurricane could thus result in increased particulate organic matter (POM) whose remineralization contributes to bottom water hypoxia (Wiseman et al., 1997). Meanwhile, the post-hurricane stratification recovery in the summer and fall seasons would have likely prevented oxygen ventilation to the bottom. The high respiration rate caused by resuspended POM could further lower the oxygen level (Bianucci et al., 2018). McCarthy et al. (2013) reported a post-Gustav respiration peak associated with organic matter resuspension in the bottom boundary layer. A recent numerical model study also simulated a substantial increase of near-bottom oxygen consumption due to resuspended POM remineralization during moderate resuspension events (Moriarty et al., 2018). These past studies and the new finding of this study suggest particulate matter (both organic and inorganic) dynamics might substantially contribute to bottom oxygen depletion and hypoxia development following a hurricane passage. More in situ observations of oxygen dynamics in the bottom boundary layer are needed.

4.3 The post-hurricane offshore bloom

Post-hurricane blooms have been widely observed in the mid- and low-latitude oceans (Davis and Yan, 2004; Miller et al., 2006; Pan et al., 2017; D'Sa et al. 2019). A bloom in the open ocean was usually isolated and patchy, and its formation was mainly related to nutrients supplied from deep waters via vertical mixing (Walker et al., 2005; Pan et al., 2017). The mechanism of the bloom formation on the outer shelf, however, was more complex due to possible impacts from the inner shelf water. Strong post-Gustav cross-shelf transport has been reported by previous studies (Korobkin et al., 2009; Zang et al., 2018). The seaward dispersal of higher nutrient and chlorophyll coastal waters could have potentially contributed to the outer shelf bloom, but their respective contributions remained unclear. To quantify the cross-shore exported nutrient and chlorophyll, we estimated depth-integrated offshore (seaward) NO_3 and chlorophyll flux along the 50 m isobath transect (Fig. 1b; Table 1). Compared with test 1 (NO_3: 7.35 mmol N/m/s; chlorophyll: 66.88 mg/m/s), the benchmark run estimated a higher NO_3 flux (38.71 mmol N/m/s) and a lower chlorophyll flux (43.10 mg/m/s). The differences in NO_3 and chlorophyll fluxes between the two simulations could be explained by nutrient accumulation and NPP reduction on the inner shelf associated with resuspended sediment (Figs. 5a and 5c). Given the better offshore bloom intensity reproduced by the benchmark run (Figs. 3d and 3e), we conclude the post-hurricane offshore bloom was mainly triggered by nutrient exported from the inner shelf water.

4.4 Sensitivity to sediment light attenuation coefficient (α_{sed})

A wide range of particle physical properties (e.g., size, shape, roughness and color) influence sediment light attenuation efficiency, which contributes to the difficulty in

parameterization of α_{sed} over a large region such as the nGoM (Baker and Lavelle, 1984; Storlazzi et al., 2015). To examine the sensitivity of primary production to sediment light attenuation efficiency, the results of sensitivity tests with different α_{sed} (tests 2–5) were compared against the benchmark run.

Ahead of Gustav's landfall, the difference in primary production between the benchmark run and sensitivity tests was limited (Fig. 8a), which suggested that the nGoM ecosystem was mainly limited by nutrient rather than light (Fennel et al., 2011). Two days after the landfall (September 1st – 3rd), high SSC suppressed photosynthesis in the entire water column which overwhelmed the response associated with different α_{sed} settings. As such, primary production was not sensitive to α_{sed} from September 1st to 3rd, although the nGoM ecosystem was also light limited. After September 3rd, the differences in primary production and NO_3 concentration increased among the sensitivity tests through September 8th (Fig. 8). Primary production became more sensitive to α_{sed} than SSC, which largely decreased due to settling (Fig. 5d). In the last two days of our simulation, the primary production differences reduced again to pre-hurricane conditions as the nGoM ecosystem shifted back to a nutrient-limited system.

In general, the influence of α_{sed} is significant when underwater light is limited by sediment and SSC was moderately high. The optical environment over the muddy inner Louisiana shelf is dominated by CDOM and chlorophyll under normal condition (D'Sa and Miller, 2003). During energetic events (e.g., hurricanes, cold fronts), however, high concentrations of resuspended sediment become the most important light absorber. Given the high frequency of cold fronts in winter (once every 3–7 days) and energetic hurricanes in summer (Walker and Hammack, 2000; Keim et al., 2007), it is reasonable to speculate that the ecosystem along coastal Louisiana would be sensitive to α_{sed} not only on event scale, but also on seasonal to annual scales. The role of long-term sediment dynamics in water clarity and marine ecology has been reported in other regions (Dupont and Aksnes, 2013; Capuzzo et al., 2015; Wilson and Heath, 2019). To prove this hypothesis in the nGoM, we need a long-term biogeochemical simulation that explicitly include sediment-induced light attenuation effects in the future.

4.5 Model uncertainties

The optical environment over the muddy Louisiana shelf is dominated by phytoplankton, suspended sediment, CDOM, and detritus particle (Le et al., 2014). The model presented in this study only includes the light attenuation due to the former two constituents, and the potential influence from CDOM and detritus warrants future study. Light attenuation due to CDOM was simply parameterized using salinity in a previous model study (Justić and Wang, 2014), yet few biogeochemical models incorporate dissolved/detritus-induced light attenuation. In the nGoM, CDOM plays an indispensable role in modulating optical properties of inner shelf waters (D'Sa and Miller, 2003; D'Sa et al. 2018), thus including CDOM-induced light attenuation would likely lower the threshold of sediment resuspension above which the nGoM ecosystem would be light-limited. To estimate the importance of CDOM-induced light attenuation in the biogeochemical models, a long-term CDOM climatology is desired in the future.

We use SeaWiFS-derived chlorophyll concentration to evaluate model performance. However, deriving high quality chlorophyll data during hurricanes is still a challenge because: 1) the presence of thick clouds limits the availability and quality of satellite images (Huang et al., 2011); 2) the uncertainty of chlorophyll estimation can be amplified by strong CDOM absorption (D'Sa and Miller, 2003; D'Sa et al., 2006); and 3) conducting chlorophyll measurements during a hurricane to calibrate bio-optical algorithms is limited by cost and safety. Given the rapid change

and a wide range of sediment and chlorophyll concentrations after hurricanes, the algorithms based on observations under normal conditions might incur a bias. To achieve a high-quality satellite-derived chlorophyll data, it is essential to optimize an algorithm based on field observations during hurricane events.

In this study we simplified α_{sed} as a constant over the entire GoM. When water is highly turbid, the availability of light for photosynthesis could be more related to sediment concentration rather than α_{sed} (McSweeney et al., 2017). Thus, using a constant to represent the sediment light attenuation coefficient when sediment concentration is high should not introduce considerable bias. The optical characteristics of sediment particles, however, could greatly modify light availability underwater when SSC is relatively low (Storlazzi et al., 2015). Our sensitivity tests also suggest the importance of α_{sed} in photosynthesis and primary production as resuspended sediment settle back to the sea floor. Therefore, it is necessary to develop a spatially explicit α_{sed} to better parameterize the sediment's impact on light attenuation in future work.

Organic matter remineralization in sediment can dramatically increase nutrient concentration in the bottom boundary layer during strong resuspension (Couceiro et al., 2013). Field measurements after hurricanes Gustav and Ike suggested that the resuspension can expose the organic material in sediment to a more favorable environment for respiration (McCarthy et al., 2013). Nevertheless, so far most biogeochemical models either neglect or simply parameterize this process (Fennel et al., 2006; Chai et al., 2007; Kishi et al., 2007). Moriarty et al. (2018) developed a particulate organic matter resuspension model and found remineralization intensity increased by an order of magnitude during moderate resuspension events in the nGoM. Given the strong storm-driven resuspension during hurricanes, nutrient dynamics can be modified greatly by remineralization after the storm passage as well. Thus, incorporating organic matter resuspension and remineralization, in conjunction with the light attenuation effects addressed in this study, will help to improve our understanding of hurricane's impact on the biogeochemical cycling in shelf waters.

Our biogeochemical model include freshwater and terrestrial nutrient input via river channel. Du et al. (2019) estimated freshwater budget during hurricane Harvey and found that surface runoff and groundwater accounted for ~34% of the total freshwater load during the hurricane. Although our understanding of nutrient flux associated with these two types of freshwater inputs is still limited, excluding surface runoff and groundwater flux in the model implies our underestimation of terrestrial nutrient discharge from the land. Coupling groundwater and hydrology models with ocean model is a feasible way to achieve a comprehensive assessment of a hurricane's impact on the coastal and shelf ecosystem. In addition, water heating due to light absorption can also impact the ecosystem (Cahill et al., 2008; Mobley et al., 2015), but it has yet to be considered in our model.

5 Conclusions

We introduced a sediment-induced light attenuation algorithm to ROMS' biogeochemical model. The new model reproduced the biogeochemical cycling during hurricane Gustav in the northern Gulf of Mexico. Improved model performance suggested suspended sediment can play an important role in underwater optical environment and primary production. During the passage of Gustav, the high SSC changed the inner shelf from a nutrient-limited environment to a light-limited one. NPP reduced from 0.05 to 0.01 g C/m^2/hr, then recovered to pre-hurricane condition after one week of hurricane landfall. As sediment further settled back on the seabed, nutrient accumulation and increased light availability incurred a strong surface post-hurricane bloom on

the inner shelf. Nine days after Gustav's arrival, NPP below 20 m water depth was still light-limited due to slow settling of sediment. The post-hurricane bloom on the outer shelf was significantly enhanced by the laterally transported nutrient from inner to outer shelf. Suspended sediment affected primary production when SSC was moderately high after Gustav's landfall. For aquatic environments with great spatiotemporal variation of SSC (e.g., estuaries and lagoons), an optimal parameterization of sediment-induced light attenuation is imperative to better evaluate hurricane's impact on coastal productivity and biogeochemical cycling.

Acknowledgements

This study was supported by NSF CyberSEES Award CCF-1856359, NASA (award number NNH17ZHA002C), Louisiana Board of Regents (award number NASA/LEQSF(2018-20)-Phase3-11), NSF Coastal SEES Award 1427389, and the LSU Foundation Billy and Ann Harrison Endowment for Sedimentary Geology. Computational support was provided by the High Performance Computing Facility (cluster Supermike II) at Louisiana State University. Model results used in this study are available at LSU mass storage system and details are on the webpage of the Coupled Ocean Modeling Group at LSU (http://www.oceanography.lsu.edu/xuelab). Data requests can be sent to the corresponding author via this webpage.

References

Allison, M.A., Demas, C.R., Ebersole, B.A., Kleiss, B.A., Little, C.D., Meselhe, E.A., Powell, N.J., Pratt, T.C., Vosburg, B.M., 2012. A water and sediment budget for the lower Mississippi-Atchafalaya River in flood years 2008-2010: Implications for sediment discharge to the oceans and coastal restoration in Louisiana. J. Hydrol. 432–433, 84–97. https://doi.org/10.1016/j.jhydrol.2012.02.020

Arndt, S., Vanderborght, J., Regnier, P., 2007. Diatom growth response to physical forcing in a macrotidal estuary: Coupling hydrodynamics, sediment transport, and biogeochemistry. J. Geophys. Res. Ocean. 112.

Baker, E.T., Lavelle, J.W., 1984. Effect of Particle Size on the Light Attenuation Coefficient of Natural Suspensions. J. Geophys. Res. 89, 8197–8203. https://doi.org/10.1029/JC089iC05p08197

Bianucci, L., Balaguru, K., Smith, R.W., Leung, L.R., Moriarty, J.M., 2018. Contribution of hurricane-induced sediment resuspension to coastal oxygen dynamics. Sci. Rep. 8. https://doi.org/10.1038/s41598-018-33640-3

Bierman, V.J., Hinz, S.C., Zhu, D., Wiseman, W.J., Rabalais, N.N., Turner, R.E., 1994. A preliminary mass balance model of primary productivity and dissolved oxygen in the Mississippi River plume/inner Gulf Shelf region. Estuaries 17, 886–899.

Booij, N., Ris, R.C., Holthuijsen, L.H., 1999. A third-generation wave model for coastal regions: 1. Model description and validation. J. Geophys. Res. Ocean. 104, 7649–7666.

Cahill, B., Schofield, O., Chant, R., Wilkin, J., Hunter, E., Glenn, S., Bissett, P., 2008. Dynamics of turbid buoyant plumes and the feedbacks on near-shore biogeochemistry and physics. Geophys. Res. Lett. 35, 1–6. https://doi.org/10.1029/2008GL033595

Capuzzo, E., Stephens, D., Silva, T., Barry, J., Forster, R.M., 2015. Decrease in water clarity of the southern and central North Sea during the 20th century. Glob. Chang. Biol. 21, 2206–2214. https://doi.org/10.1111/gcb.12854

Chai, F., Jiang, M.S., Chao, Y., Dugdale, R.C., Chavez, F., Barber, R.T., 2007. Modeling

responses of diatom productivity and biogenic silica export to iron enrichment in the equatorial Pacific Ocean. Global Biogeochem. Cycles 21, 1–16. https://doi.org/10.1029/2006GB002804

Cloern, J.E., 1987. Turbidity as a control on phytoplankton biomass and productivity in estuaries. Cont. Shelf Res. 7, 1367–1381.

Couceiro, F., Fones, G.R., Thompson, C.E.L., Statham, P.J., Sivyer, D.B., Parker, R., Kelly-Gerreyn, B.A., Amos, C.L., 2013. Impact of resuspension of cohesive sediments at the Oyster Grounds (North Sea) on nutrient exchange across the sediment-water interface. Biogeochemistry 113, 37–52. https://doi.org/10.1007/s10533-012-9710-7

D'Sa, E.J., Korobkin, M., Ko, D.S., 2011. Effects of Hurricane Ike on the Louisiana-Texas coast from satellite and model data. Remote Sens. Lett. 2, 11–19. https://doi.org/10.1080/01431161.2010.489057

D'Sa, E.J., Miller, R.L., 2003. Bio-optical properties in waters influenced by the Mississippi River during low flow conditions. Remote Sens. Environ. 84, 538–549. https://doi.org/10.1016/S0034-4257(02)00163-3

D'Sa, E.J., Miller, R.L., Del Castillo, C., 2006. Bio-optical properties and ocean color algorithms for coastal waters influenced by the Mississippi River during a cold front. Appl. Opt. 45, 7410–7428.

D'Sa, E.J., Joshi, I.D., Liu, B., 2018. Galveston Bay and coastal ocean optical-geochemical response to Hurricane Harvey from VIIRS ocean color. Geophys. Res. Lett. 45, https://doi.org/10.1029/2018GL079954

D'Sa, E.J., Joshi, I.D., Liu, B., Ko, D.S., Osburn, C.L., Bianchi, T.S., 2019. Biogeochemical response of Apalachicola Bay and the shelf waters to Hurricane Michael using ocean color semi-analytic/inversion and hydrodynamic models. Front. Mar. Sci. 6:523, doi:10.3389/fmars.2019.00523

Davis, A., Yan, X.H., 2004. Hurricane forcing on chlorophyll-a concentration off the northeast coast of the U.S. Geophys. Res. Lett. 31, 4–7. https://doi.org/10.1029/2004GL020668

Devlin, M.J., Barry, J., Mills, D.K., Gowen, R.J., Foden, J., Sivyer, D., Tett, P., 2008. Relationships between suspended particulate material, light attenuation and Secchi depth in UK marine waters. Estuar. Coast. Shelf Sci. 79, 429–439. https://doi.org/10.1016/j.ecss.2008.04.024

Du, J., Park, K., Dellapenna, T.M., Clay, J.M., 2019. Dramatic hydrodynamic and sedimentary responses in Galveston Bay and adjacent inner shelf to Hurricane Harvey. Sci. Total Environ. 653, 554–564. https://doi.org/10.1016/j.scitotenv.2018.10.403

Dupont, N., Aksnes, D.L., 2013. Centennial changes in water clarity of the baltic sea and the north sea. Estuar. Coast. Shelf Sci. 131, 282–289. https://doi.org/10.1016/j.ecss.2013.08.010

Fennel, K., Hetland, R., Feng, Y., Dimarco, S., 2011. A coupled physical-biological model of the Northern Gulf of Mexico shelf: Model description, validation and analysis of phytoplankton variability. Biogeosciences 8, 1881–1899. https://doi.org/10.5194/bg-8-1881-2011

Fennel, K., Wilkin, J., Levin, J., Moisan, J., O'Reilly, J., Haidvogel, D., 2006. Nitrogen cycling in the Middle Atlantic Bight: Results from a three-dimensional model and implications for the North Atlantic nitrogen budget. Global Biogeochem. Cycles 20, 1–14. https://doi.org/10.1029/2005GB002456

Fennel, K., Wilkin, J., Previdi, M., Najjar, R., 2008. Denitrification effects on air-sea CO2 flux in the coastal ocean: Simulations for the northwest North Atlantic. Geophys. Res. Lett. 35, 1–5. https://doi.org/10.1029/2008GL036147

Forbes, C., Luettich, R. a., Mattocks, C. a., Westerink, J.J., 2010. A Retrospective Evaluation of the Storm Surge Produced by Hurricane Gustav (2008): Forecast and Hindcast Results. Weather Forecast. 25, 1577–1602. https://doi.org/10.1175/2010WAF2222416.1

Ganju, N.K., Miselis, J.L., Aretxabaleta, A.L., 2014. Physical and biogeochemical controls on light attenuation in a eutrophic, back-barrier estuary. Biogeosciences 11, 7193–7205. https://doi.org/10.5194/bg-11-7193-2014

Gomez, F.A., Lee, S.K., Liu, Y., Hernandez, F.J., Muller-Karger, F.E., Lamkin, J.T., 2018. Seasonal patterns in phytoplankton biomass across the northern and deep Gulf of Mexico: A numerical model study. Biogeosciences 15, 3561–3576. https://doi.org/10.5194/bg-15-3561-2018

Haidvogel, D.B., Arango, H., Budgell, W.P., Cornuelle, B.D., Curchitser, E., Di Lorenzo, E., Fennel, K., Geyer, W.R., Hermann, A.J., Lanerolle, L., Levin, J., McWilliams, J.C., Miller, A.J., Moore, A.M., Powell, T.M., Shchepetkin, A.F., Sherwood, C.R., Signell, R.P., Warner, J.C., Wilkin, J., 2008. Ocean forecasting in terrain-following coordinates: Formulation and skill assessment of the Regional Ocean Modeling System. J. Comput. Phys. 227, 3595–3624. https://doi.org/10.1016/j.jcp.2007.06.016

Huang, W., Mukherjee, D., Chen, S., 2011. Assessment of Hurricane Ivan impact on chlorophyll-a in Pensacola Bay by MODIS 250m remote sensing. Mar. Pollut. Bull. 62, 490–498. https://doi.org/10.1016/j.marpolbul.2010.12.010

Hurst, N.R., White, J.R., Xu, K., Ren, M., 2019. Nitrate reduction rates in sediments experiencing turbulent flow conditions. Ecol. Eng. 128, 33–38. https://doi.org/10.1016/j.ecoleng.2018.12.027

Jacob, R., Larson, J., Everest, O., 2005. M x N Communication and Parallel Interpolation in Community Climate System Model Version 3 Using the Model Coupling Toolkit. Int. J. High Perform. Comput. Appl. 19, 293–307. https://doi.org/10.1177/1094342005056116

Justić, D., Wang, L., 2014. Assessing temporal and spatial variability of hypoxia over the inner Louisiana-upper Texas shelf: Application of an unstructured-grid three-dimensional coupled hydrodynamic-water quality model. Cont. Shelf Res. 72, 163–179. https://doi.org/10.1016/j.csr.2013.08.006

Keim, B.D., Muller, R.A., Stone, G.W., 2007. Spatiotemporal patterns and return periods of tropical storm and hurricane strikes from Texas to Maine. J. Clim. 20, 3498–3509. https://doi.org/10.1175/JCLI4187.1

Kishi, M.J., Kashiwai, M., Ware, D.M., Megrey, B.A., Eslinger, D.L., Werner, F.E., Noguchi-Aita, M., Azumaya, T., Fujii, M., Hashimoto, S., 2007. NEMURO—a lower trophic level model for the North Pacific marine ecosystem. Ecol. Modell. 202, 12–25.

Korobkin, M., D'Sa, E., Ko, D.S., 2009. Satellite observations and NCOM assessment of the Mississippi-Louisiana-Texas coast following hurricanes Gustav and Ike. Ocean. 2009 1–4. https://doi.org/10.23919/OCEANS.2009.5422213

Laurent, A., Fennel, K., 2014. Simulated reduction of hypoxia in the northern Gulf of Mexico due to phosphorus limitation. Elementa 2, 1–12. https://doi.org/10.12952/journal.elementa.000022

Laurent, A., Fennel, K., Hu, J., Hetland, R., 2012. Simulating the effects of phosphorus limitation in the Mississippi and Atchafalaya river plumes. Biogeosciences 9, 4707–4723. https://doi.org/10.5194/bg-9-4707-2012

Le, C., Lehrter, J.C., Hu, C., Murrell, M.C., Qi, L., 2014. Spatiotemporal chlorophyll-a dynamics on the Louisiana continental shelf derived from a dual satellite imagery algorithm. J.

529 Geophys. Res. Ocean. 119, 7449–7462.
530 Lin, S., Zou, T., Gao, H., Guo, X., 2009. The vertical attenuation of irradiance as a function of
531 turbidity: a case of the Huanghai (Yellow) Sea in spring. Acta Oceanol. Sin. 28, 66–75.
532 Liu, K., Chen, Q., Hu, K., Xu, K., Twilley, R.R., 2018. Modeling hurricane-induced wetland-bay
533 and bay-shelf sediment fluxes. Coast. Eng. 135, 77–90.
534 https://doi.org/10.1016/j.coastaleng.2017.12.014
535 McCarthy, M.J., Carini, S.A., Liu, Z., Ostrom, N.E., Gardner, W.S., 2013. Oxygen consumption
536 in the water column and sediments of the northern Gulf of Mexico hypoxic zone. Estuar.
537 Coast. Shelf Sci. 123, 46–53. https://doi.org/10.1016/j.ecss.2013.02.019
538 McSweeney, J.M., Chant, R.J., Wilkin, J.L., Sommerfield, C.K., 2017. Suspended-Sediment
539 Impacts on Light-Limited Productivity in the Delaware Estuary. Estuaries and Coasts 40,
540 977–993. https://doi.org/10.1007/s12237-016-0200-3
541 Meade, R.H., Moody, J.A., 2010. Causes for the decline of suspended-sediment discharge in the
542 Mississippi River system, 1940-2007. Hydrol. Process. 24, 35–49.
543 Miller, W.D., Harding, L.W., Adolf, J.E., 2006. Hurricane Isabel generated an unusual fall
544 bloom in Chesapeake Bay. Geophys. Res. Lett. 33, 2–5.
545 https://doi.org/10.1029/2005GL025658
546 Mobley, C.D., Chai, F., Xiu, P., Sundman, L.K., 2015. Impact of improved light calculations on
547 predicted phytoplankton growth and heating in an idealized upwelling-downwelling channel
548 geometry. J. Geophys. Res. Ocean. 120, 875–892.
549 Moriarty, J.M., Harris, C.K., Fennel, K., Friedrichs, M.A.M., Xu, K., Rabouille, C., 2017. The
550 roles of resuspension, diffusion and biogeochemical processes on oxygen dynamics
551 offshore of the Rhône River, France: A numerical modeling study. Biogeosciences 14,
552 1919–1946. https://doi.org/10.5194/bg-14-1919-2017
553 Moriarty, J.M., Harris, C.K., Friedrichs, M.A.M., Fennel, K., Xu, K., 2018. Impact of seabed
554 resuspension on oxygen and nitrogen dynamics in the northern Gulf of Mexico: A
555 numerical modeling study. J. Geophys. Res. Ocean. 1–27.
556 https://doi.org/10.1029/2018JC013950
557 Pan, G., Chai, F., Tang, D.L., Wang, D., 2017. Marine phytoplankton biomass responses to
558 typhoon events in the South China Sea based on physical-biogeochemical model. Ecol.
559 Modell. 356, 38–47. https://doi.org/10.1016/j.ecolmodel.2017.04.013
560 Pennock, J.R., 1985. Chlorophyll distributions in the Delaware estuary: regulation by light-
561 limitation. Estuar. Coast. Shelf Sci. 21, 711–725.
562 Rabalais, N.N., Turner, R.E., Wiseman, W.J., 2001. Hypoxia in the Gulf of Mexico. J. Environ.
563 Qual. 30, 320–329.
564 Saha, S., Moorthi, S., Pan, H.L., Wu, X., Wang, J., Nadiga, S., Tripp, P., Kistler, R., Woollen, J.,
565 Behringer, D., 2010. NCEP climate forecast system reanalysis (CFSR) 6-hourly products,
566 January 1979 to December 2010. Res. Data Arch. Natl. Cent. Atmos. Res. Comput. Inf.
567 Syst. Lab. Boulder, CO.
568 Saha, S., Moorthi, S., Wu, X., Wang, J., Nadiga, S., Tripp, P., Behringer, D., Hou, Y.T., Chuang,
569 H., Iredell, M., 2011. NCEP climate forecast system version 2 (CFSv2) 6-hourly products.
570 Res. Data Arch. Natl. Cent. Atmos. Res. Comput. Inf. Syst. Lab.
571 Schaeffer, B.A., Sinclair, G.A., Lehrter, J.C., Murrell, M.C., Kurtz, J.C., Gould, R.W., Yates,
572 D.F., 2011. An analysis of diffuse light attenuation in the northern Gulf of Mexico hypoxic
573 zone using the SeaWiFS satellite data record. Remote Sens. Environ. 115, 3748–3757.
574 https://doi.org/10.1016/j.rse.2011.09.013

Shchepetkin, A.F., McWilliams, J.C., 2005. The regional oceanic modeling system (ROMS): A split-explicit, free-surface, topography-following-coordinate oceanic model. Ocean Model. 9, 347–404. https://doi.org/10.1016/j.ocemod.2004.08.002

Skamarock, W.C., Klemp, J.B., Dudhi, J., Gill, D.O., Barker, D.M., Duda, M.G., Huang, X.-Y., Wang, W., Powers, J.G., 2005. A Description of the Advanced Research WRF Version 3. Tech. Rep. 113. https://doi.org/10.5065/D6DZ069T

Storlazzi, C.D., Norris, B.K., Rosenberger, K.J., 2015. The influence of grain size, grain color, and suspended-sediment concentration on light attenuation: Why fine-grained terrestrial sediment is bad for coral reef ecosystems. Coral Reefs 34, 967–975. https://doi.org/10.1007/s00338-015-1268-0

Thewes, D., Stanev, E. V., Zielinski, O., 2020. Sensitivity of a 3D Shelf Sea Ecosystem Model to Parameterizations of the Underwater Light Field. Front. Mar. Sci. 6. https://doi.org/10.3389/fmars.2019.00816

Tweel, A.W., Turner, R.E., 2012. Landscape-Scale Analysis of Wetland Sediment Deposition from Four Tropical Cyclone Events. PLoS One 7. https://doi.org/10.1371/journal.pone.0050528

Walker, N.D., Hammack, A.B., 2000. Impacts of winter storms on circulation and sediment transport: Atchafalaya-Vermilion Bay region, Louisiana, USA. J. Coast. Res. 16, 996–1010. https://doi.org/10.2307/4300118

Walker, N.D., Leben, R.R., Balasubramanian, S., 2005. Hurricane-forced upwelling and chlorophyll a enhancement within cold-core cyclones in the Gulf of Mexico. Geophys. Res. Lett. 32, 1–5. https://doi.org/10.1029/2005GL023716

Warner, J.C., Armstrong, B., He, R., Zambon, J.B., 2010. Development of a Coupled Ocean-Atmosphere-Wave-Sediment Transport (COAWST) Modeling System. Ocean Model. 35, 230–244. https://doi.org/10.1016/j.ocemod.2010.07.010

Warner, J.C., Sherwood, C.R., Signell, R.P., Harris, C.K., Arango, H.G., 2008. Development of a three-dimensional, regional, coupled wave, current, and sediment-transport model. Comput. Geosci. 34, 1284–1306. https://doi.org/10.1016/j.cageo.2008.02.012

Wilson, R.F., Fennel, K., Paul Mattern, J., 2013. Simulating sediment-water exchange of nutrients and oxygen: A comparative assessment of models against mesocosm observations. Cont. Shelf Res. 63, 69–84. https://doi.org/10.1016/j.csr.2013.05.003

Wilson, R.J., Heath, M.R., 2019. Increasing turbidity in the North Sea during the 20th century due to changing wave climate. Ocean Sci. 15, 1615–1625. https://doi.org/10.5194/os-15-1615-2019

Wiseman, W.J., Rabalais, N.N., Turner, R.E., Dinnel, S.P., MacNaughton, A., 1997. Seasonal and interannual variability within the Louisiana coastal current: stratification and hypoxia. J. Mar. Syst. 12, 237–248.

Xu, K., Harris, C.K., Hetland, R.D., Kaihatu, J.M., 2011. Dispersal of Mississippi and Atchafalaya sediment on the Texas-Louisiana shelf: Model estimates for the year 1993. Cont. Shelf Res. 31, 1558–1575. https://doi.org/10.1016/j.csr.2011.05.008

Xu, K., Mickey, R.C., Chen, Q., Harris, C.K., Hetland, R.D., Hu, K., Wang, J., 2016. Shelf sediment transport during hurricanes Katrina and Rita. Comput. Geosci. 90, 24–39. https://doi.org/10.1016/j.cageo.2015.10.009

Xue, Z., He, R., Fennel, K., Cai, W.J., Lohrenz, S., Hopkinson, C., 2013. Modeling ocean circulation and biogeochemical variability in the Gulf of Mexico. Biogeosciences 10, 7219–7234. https://doi.org/10.5194/bg-10-7219-2013

Yu, L., Fennel, K., Laurent, A., 2015. A modeling study of physical controls on hypoxia generationin the northern Gulf of Mexico. J. Geophys. Res. Ocean. 1–16. https://doi.org/10.1002/2014JC010472.Received

Zang, Z., Xue, Z.G., Bao, S., Chen, Q., Walker, N.D., Haag, A.S., Ge, Q., Yao, Z., 2018. Numerical study of sediment dynamics during hurricane Gustav. Ocean Model. 126, 29–42. https://doi.org/10.1016/j.ocemod.2018.04.002

Zang, Z., Xue, Z.G., Xu, K., Bentley, S.J., Chen, Q., D'Sa, E.J., Ge, Q., 2019. A Two Decadal (1993–2012) Numerical Assessment of Sediment Dynamics in the Northern Gulf of Mexico. Water 11, 938.

Zhao, Y., Quigg, A., 2014. Nutrient limitation in Northern Gulf of Mexico (NGOM): Phytoplankton communities and photosynthesis respond to nutrient pulse. PLoS One 9. https://doi.org/10.1371/journal.pone.0088732

Zhou, F., Chai, F., Huang, D., Xue, H., Chen, J., Xiu, P., Xuan, J., Li, J., Zeng, D., Ni, X., Wang, K., 2017. Investigation of hypoxia off the Changjiang Estuary using a coupled model of ROMS-CoSiNE. Prog. Oceanogr. 159, 237–254. https://doi.org/10.1016/j.pocean.2017.10.008

Zhu, Z., Ng, W., Liu, S., Zhang, J., Chen, J., Wu, Y., 2009. Estuarine phytoplankton dynamics and shift of limiting factors: A study in the Changjiang (Yangtze River) Estuary and adjacent area. Estuar. Coast. Shelf Sci. 84, 393–401.

Figure 1. panel a: Model domains applied in this study. The entire panel a is the WRF model domain (6 km resolution) overlaid with water depth (color-shading). The black solid box represents the model grid used by ROMS and SWAN with 5 km resolution. The black dashed line box (lat: 27°N–31°N; lon: 94°W–86°W) covers the northern Gulf of Mexico (nGoM). More details in the nGoM are shown in panel b. The thick purple/red lines indicate locations of 50m-isobath transect and transect D (Rabalais et al., 2001), respectively.

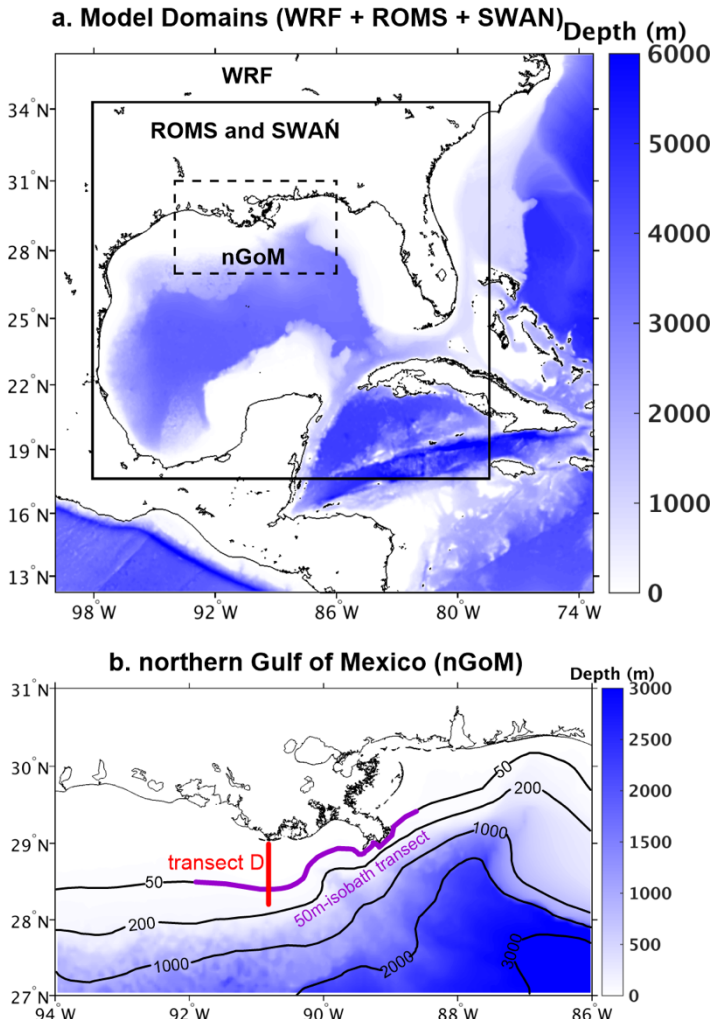

Figure 2. Flow chart of long-term (20 years) and hurricane (11 days) simulations. In Step 1 we only run ocean (ROMS) and biogeochemical (NEMURO) models, which provide initial inputs for the next step. Step 2 couples ocean (ROMS), wave (SWAN), atmosphere (WRF), sediment (CSTMS) and new biogeochemical (NEMURO) models with new sediment-induced light attenuation term.

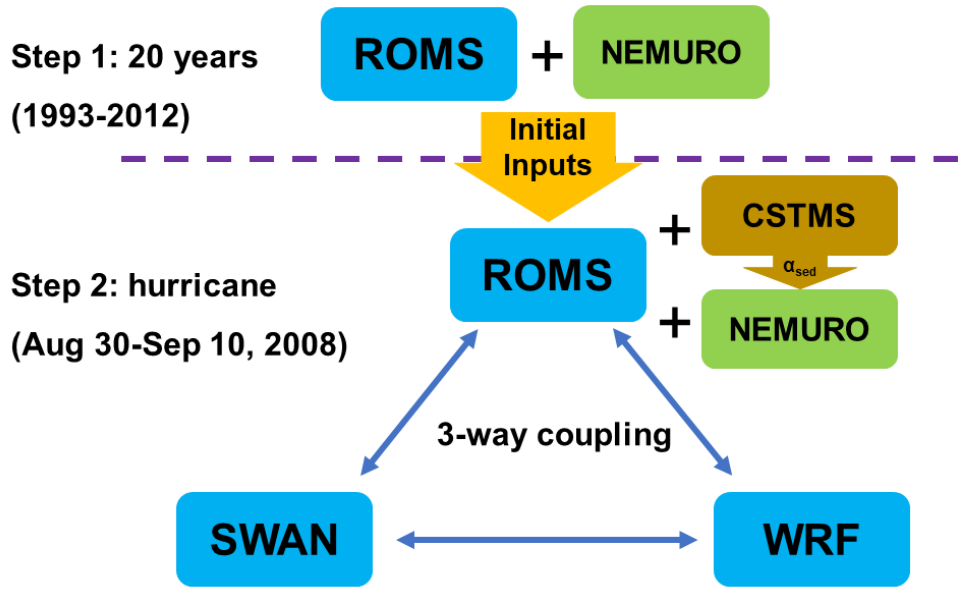

Figure 3. Initial condition of surface chlorophyll extracted from 20-year simulation (a) and five-day composite of surface chlorophyll concentration in the year 2008: (b) SeaWiFS data before Gustav (August 25th–29th); (c) SeaWiFS data after Gustav (September 05th–09th); (d) benchmark run result ($\alpha_{sed} = 0.059$) after Gustav; (e) test 1 result ($\alpha_{sed} = 0$) after Gustav. White color in panels (b) and (c) represents no data. Magenta curve shows hurricane track in panels b, c, and d. (BD: bird-foot Mississippi delta; AS: Atchafalaya shelf).

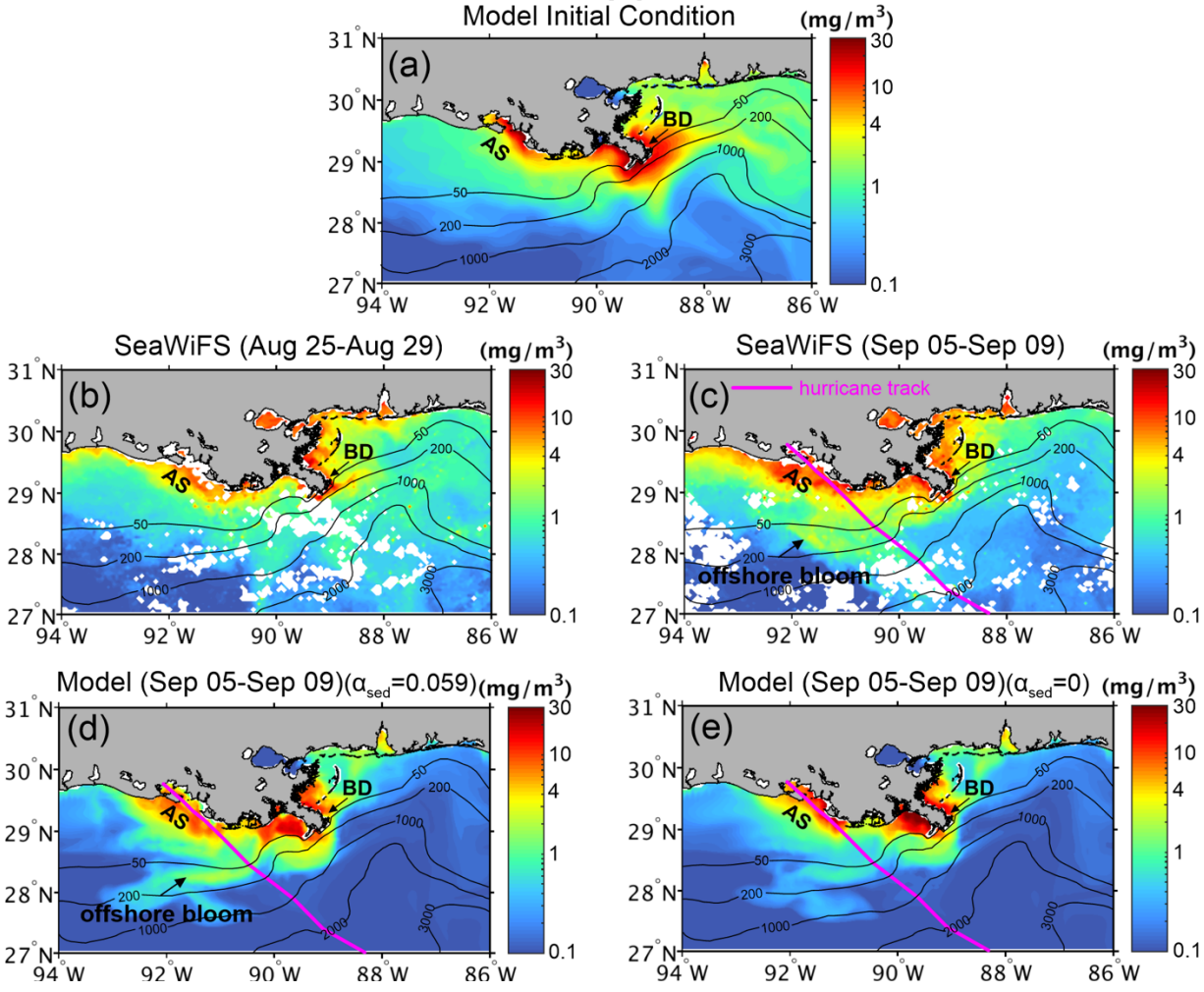

665 **Figure 4.** Simulated five-day composite (September 05th–09th) of surface chlorophyll
666 concentration after hurricane Gustav compared to corresponding SeaWiFS-derived surface
667 chlorophyll results over the nGOM inner shelf (h < 50 m) for model results based on (a)
668 benchmark ($\alpha_{sed} = 0.059$) and (b) test 1 ($\alpha_{sed} = 0$) runs.

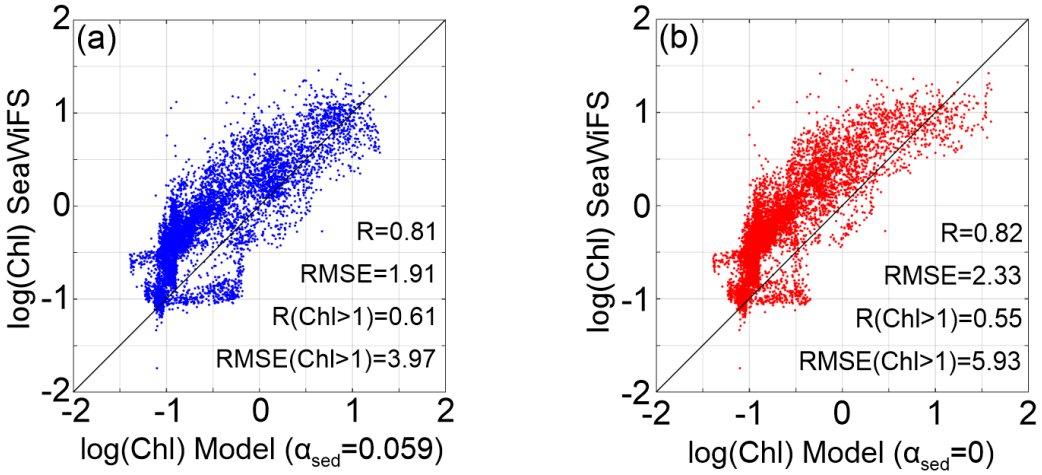

669
670

Figure 5. Time series of spatially averaged (inner shelf, water depth < 50 m) net primary production (a), surface chlorophyll concentration (b), surface NO_3 concentration (c), surface suspended sediment concentration (d), solar shortwave radiation (e), and sea surface temperature (f). In panels a, b, and c, blue represents benchmark run ($\alpha_{sed} = 0.059$) and red represents test 1 ($\alpha_{sed} = 0$). Dots in panel (a) are daily-averaged net primary production. The black dashed line shows the time of Gustav landfall.

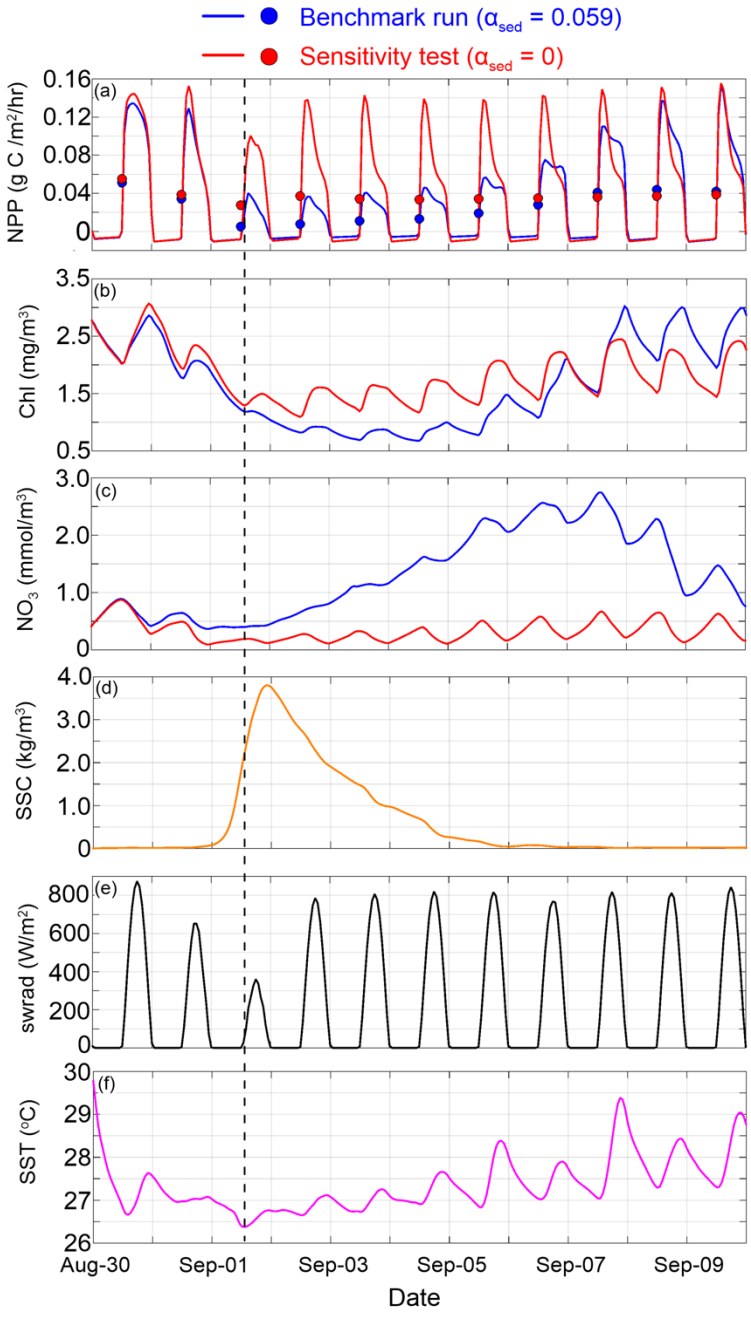

Figure 6. Model simulated chlorophyll and NO_3 along transect D on August 31st (first column), September 2nd (second column), and September 10th (third column). The first and second rows represent chlorophyll concentration of the test 1 and benchmark run, respectively (note the color scale is different from Fig. 3). The third and fourth rows show NO_3 concentration of test 1 and benchmark run, respectively.

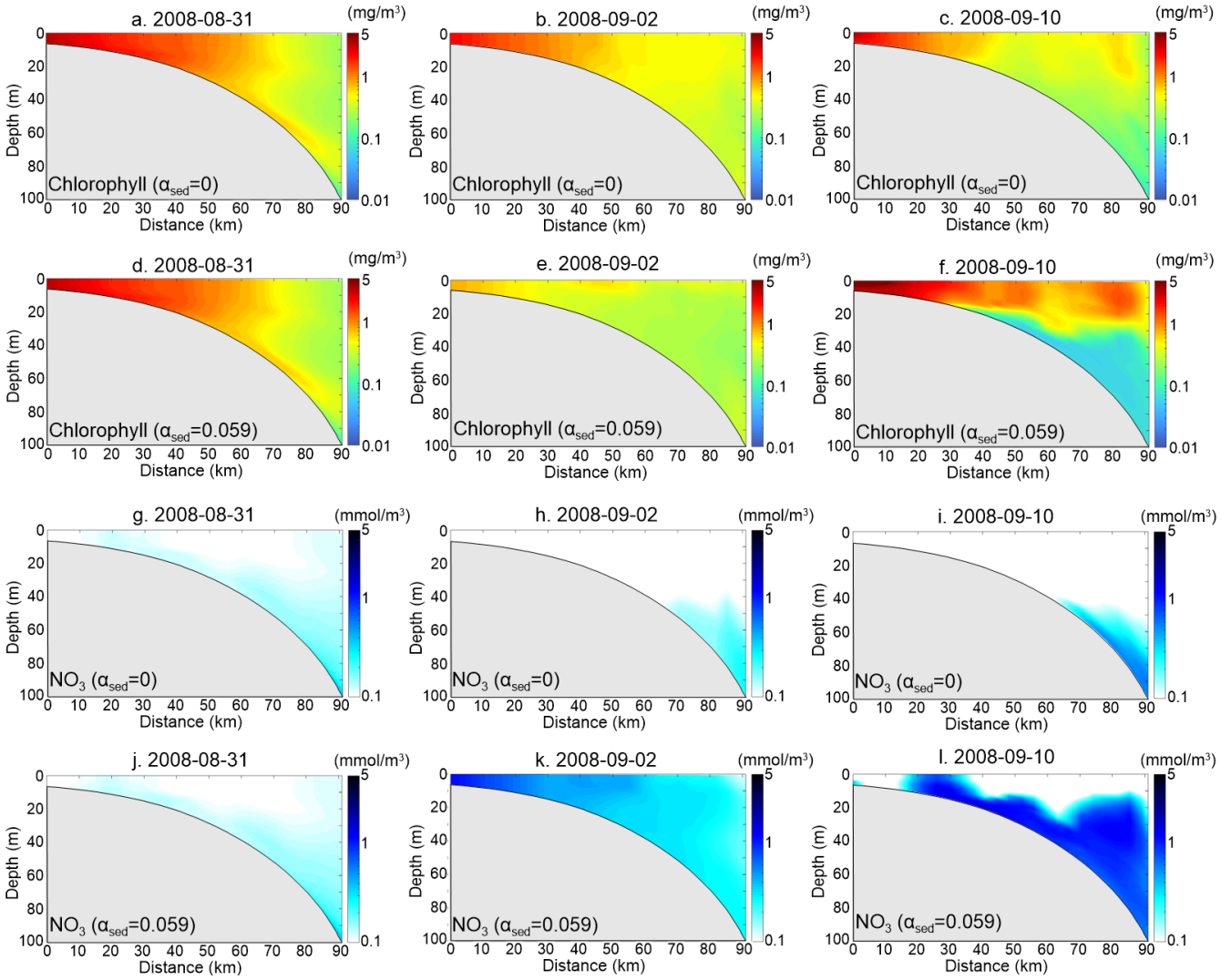

Figure 7. Model simulated suspended sediment concentration (SSC; first row) and water density anomaly (second row) along transect D on August 31st (a, d), September 2nd (b, e), and September 10th (c, f), respectively.

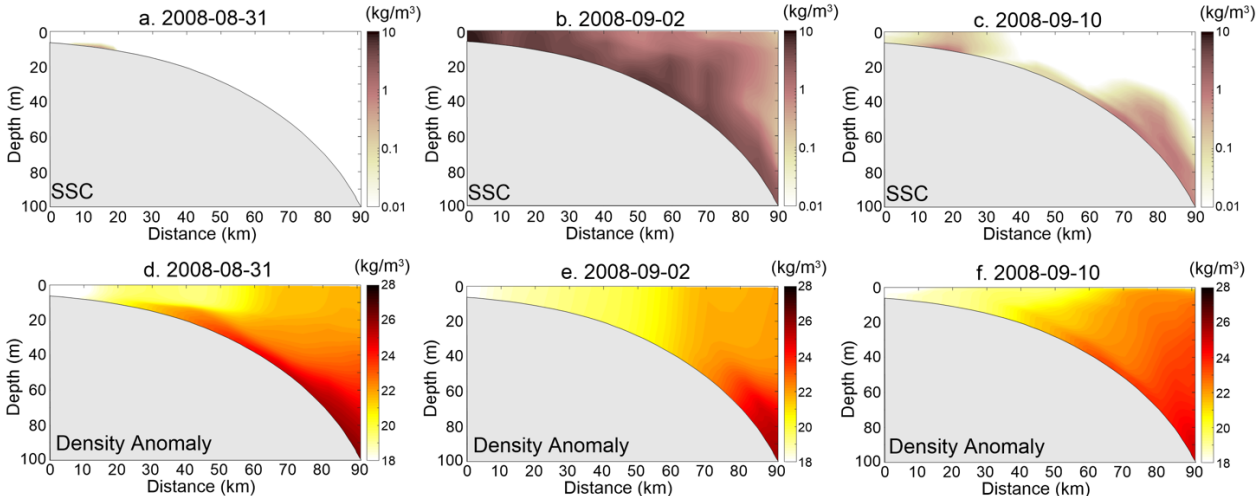

Figure 8. Comparison of spatial averaged (inner shelf, water depth < 50 m) net primary production (panel a) and NO_3 concentration (panel b) between benchmark run (blue) and sensitivity tests with different α_{sed} (test 2: cyan; test 3: orange; test 4: black; test 5: magenta). The black dashed line shows the time of Gustav landfall.

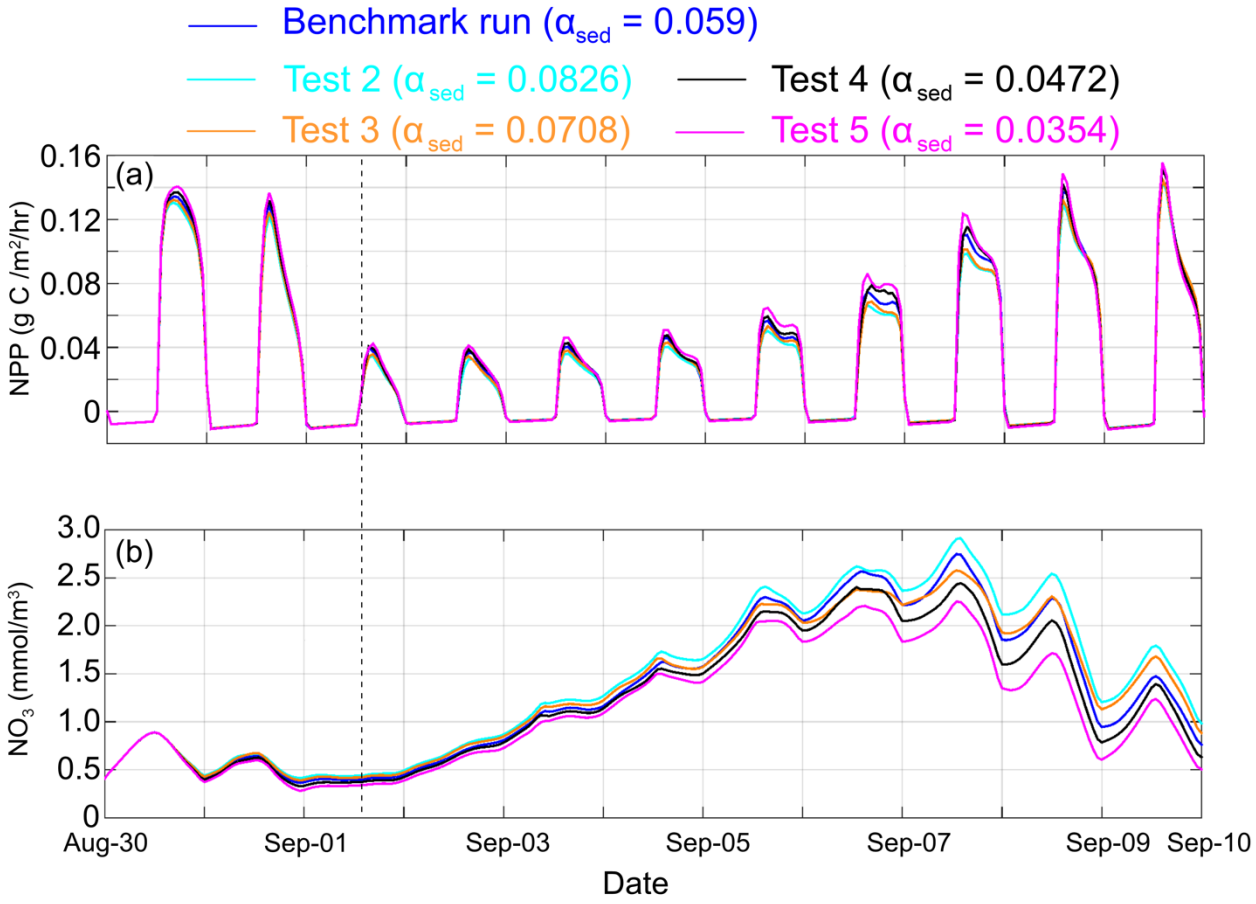

700 **Table 1.** Offshore fluxes of NO_3 and chlorophyll along the 50-m isobath transect (see location
701 in Fig. 1b).
702

Model Runs	Net offshore NO_3 flux (mmol N/m/s)	Net offshore Chl flux (mg/m/s)
benchmark run ($\alpha_{sed} = 0.059$)	38.71	43.10
test 1 ($\alpha_{sed} = 0$)	7.35	66.88

703
704